Nanoscale

Multifunctional and Flexible ZrO2-Coated EGaIn Nanoparticles for Photothermal Therapy

Journal:	*Nanoscale*
Manuscript ID	NR-COM-03-2019-001963.R1
Article Type:	Communication
Date Submitted by the Author:	17-Apr-2019
Complete List of Authors:	Xia, Na; Sichuan University Li, Na; The 304 Research Institute of China Aerospace Science and Industry Corp Rao, Wei; Technical Institute of Physics and Chemistry Yu, Jie; Chinese PLA General Hospital of Beijing Command Area Wu, Qiong; Technical Institute of Physics and Chemistry Chinese Academy of Sciences Tan, Longfei; Technical Institute of Physics and Chemistry Chinese Academy of Sciences Li, Hongbo; Beijing Institute of Technology, School of Materials Science & Engineering Gou, Li; Sichuan University, Liang, Ping; Chinese PLA General Hospital of Beijing Command Area Li, Laifeng; Technical Institute of Physics and Chemistry Chinese Academy of Sciences Meng, Xianwei; Technical Institute of Physics and Chemistry Chinese Academy of Sciences

COMMUNICATION

Multifunctional and Flexible ZrO_2-Coated EGaIn Nanoparticles for Photothermal Therapy

Received 00th January 20xx,
Accepted 00th January 20xx

DOI: 10.1039/x0xx00000x

Na Xia,[a,b] Na Li,[c] Wei Rao,*[b] Jie Yu,[d] Qiong Wu,[b] Longfei Tan,[b] Hongbo Li,[e] Li Gou,*[a] Ping Liang,[d] Laifeng Li [b] and Xianwei Meng *[b]

With the intensive study of liquid metals (LMs), Ga-based LMs attract more attention of biomedical researches for good biocompatibility, ideal fluidity and high thermal conductivity. The concern of liquid metal (LM) applied in cancer treatment is the high surface tension to form unstable nanoparticles. Here, ZrO_2 is coated on the LM nanoparticles to form a stable core-shell nanostructure. In particular, the LM nanoparticles coated with ZrO_2 and modified by PEG (LM@pZrO_2 NPs) still maintain favorable flexibility, which is beneficial for cellular uptake. With the photothermal properties of LM, LM@pZrO_2 NPs rapidly warm up and emit amount of heat under NIR laser radiation. It is confirmed that LM@pZrO_2 NPs are more effectively internalized by cells and are beneficial to tumor photothermal therapy. This research provides a coating strategy to construct a stable and flexible core-shell LM nanostructure, making it a promising vehicle for nanotheranostics.

Introduction

To date, metals and alloys with a melting point close to room temperature, called 'liquid metals' (LMs), have been widely applied in many fields such as electronics, mechanical engineering and energy.[1, 2] With the in-depth study of LMs, Ga-based LMs have attracted the attention of biomedical scholars. These LMs not only have good fluidity and high thermal conductivity, but also have good biocompatibility.[3, 4] Recently, LMs with a size of nanometer level, increasing the specific surface area and volume ratio, were applied to drug carrier, molecular imaging or cancer treatment.[5] The deformability of LMs was always used to release drugs. Lu et al. developed a transformable LMs nanoparticle that rapidly heats up and produces reactive oxygen to deform and release the drug under the NIR radiation.[6] Chechetka et al. developed a LMs nanocapsule which quickly warms up, deforms and releases the drug in near-infrared light, simultaneously produces reactive oxygen species.[7]

However, the common problem of liquid metal (LM) applied in cancer treatment is how to overcome the high surface tension to form stable nanoparticles.[8] High surface tension drives adjacent LM droplets to combine, hindering the stable formation of small size LM. Known from the literatures,[9-11] the surface properties of nanoparticles can be significantly improved with the core-shell structure in which the LM are fully encapsulated and separated into individual droplets. Inorganic nanoparticles have many advantages such as facile preparation, tailorable size, shape and surface ligands.[12, 13] Therefore, the LM nanoparticles can be stabilized by forming an inorganic shell on the outer layer.

Here, we designed a multifunctional nanoparticle with a stable core-shell structure and the ideal flexibility of LM. Moreover, LM coated with ZrO_2 has better stability in water, which is helpful for the application of LM nanoparticles in organisms. ZrO_2 was coated on the LM (EGaIn, 75.5% Ga and 24.5% In by weight) nanoparticles to form a stable nanostructure (LM@ZrO_2 NPs), and PEG was used to improve the biocompatibility of LM@pZrO_2 NPs (**Scheme 1**a). More importantly, the obtained nanoparticles maintained favorable flexibility, which was beneficial for cellular uptake. The mechanical properties of LM@ZrO_2 NPs was close to that of LM, which was significantly 'softer' than hollow ZrO_2 NPs. In cell experiment, LM@pZrO_2 NPs were confirmed to be more effectively internalized than LM NPs by HepG2 cells. LM@pZrO_2 NPs also maintained ideal photothermal (PT) conversion performance and was used for anti-tumor therapy in mice. LM@pZrO_2 NPs with ideal flexibility were effectively internalized by cells and then used in tumor photothermal

[a] College of Materials Science and Engineering, Sichuan University, Chengdu 610065 China, email: gouli@scu.edu.cn
[b] Laboratory of Controllable Preparation and Application of Nanomaterials, CAS Key, Laboratory of Cryogenics, Technical Institute of Physics and Chemistry, Chinese Academy of Sciences, 29 Zhongguancun East Road, Beijing 100190 China, email: mengxw@mail.ipc.ac.cn; weirao@mail.ipc.ac.cn
[c] The 304 Research Institute of China Aerospace Science and Industry Corp.
[d] Department of Interventional Ultrasound, Chinese PLA General Hospital, Beijing 100853 China
[e] Beijing Key Laboratory of Construction-Tailorable Advanced Functional Materials and Green Applications, School of Materials Science & Engineering, Beijing Institute of Technology, Beijing 10081 China
†Electronic Supplementary Information (ESI) available: [details of any supplementary information available should be included here]. See DOI: 10.1039/x0xx00000x

therapy (PTT) to damage cancer cells under NIR irradiation (Scheme 1b). In addition, LM@pZrO$_2$ NPs with CT imaging effects can monitor the therapeutic effects visually in real time. The core-shell LM nanostructure holds the significant advantages of stability as well as flexibility, making it a promising vehicle for nanotheranostics.

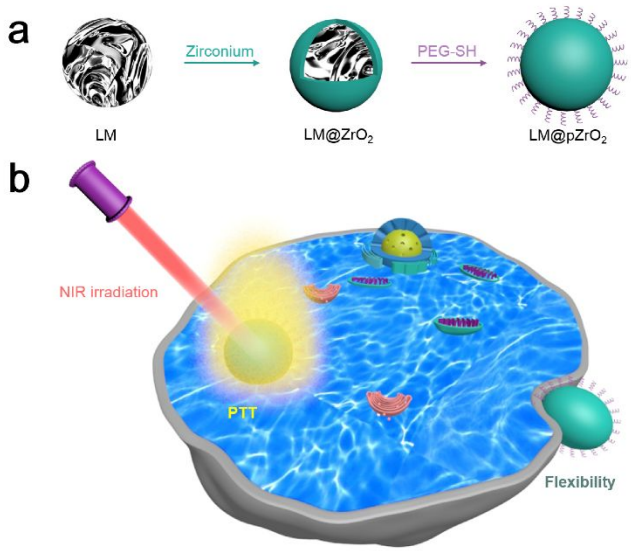

Scheme 1. Experimental diagrams. a) Schematic diagram of the synthetic route of LM@pZrO$_2$ NPs. b) Schematic diagram of LM@pZrO$_2$ NPs with ideal flexibility for photothermal therapy under NIR radiation.

Results and discussion

Synthesis and structural characterization of LM@pZrO$_2$ NPs

Our previous work found that hollow ZrO$_2$ in aqueous solution could form stable suspensions.[14] It is speculated that stable LM particles could be formed by encapsulating the ZrO$_2$ shell on the surface of LM particles to prevent LM from re-aggregation. LM@ZrO$_2$ NPs was prepared through simple methods at room temperature. Firstly, the suspension of EGaIn was dispersed in mixture of ethanol and span85 by ultrasound. Then, acetonitrile and ammonia were immersed in the mixed solution. Next, zirconium n-propoxide was stirred in the mixed solution with a magnetic stirrer and hydrolyzed to ZrO$_2$ in the presence of ammonia. So ZrO$_2$ was coated on the outer layer of LM to form a core-shell structure around LM nanoparticles. As shown in **Figure 1**a, the surface morphology of LM@ZrO$_2$ NPs with the sphere was observed by the characterization of SEM. Their particle size was about 120 ± 60 nm using the counting software of Nano Measurer. Spherical core-shell structures were displayed by TEM analysis (Figure 1b). Furthermore, EDS results showed that the elements of nuclear layer were mainly Ga and In, while the shell was mainly Zr and O (Figure 1c, d), demonstrating LM was successfully wrapped by the ZrO$_2$ shell. The dynamics diameter of LM@ZrO$_2$ NPs was around 119 nm measured with Malvern nanoZSE with dispersity of 0.105, suggesting good dispersion stability (Figure S1a). We believe that this shell can effectively prevent size change and reversible aggregation of LM particles. The stability of LM@ZrO$_2$ was also studied by dispersing LM@ZrO$_2$ NPs and LM NPs in water. LM NPs completely settled within 1 h, but LM@ZrO$_2$ NPs were stably dispersed in water without any change (Figure S2). In the next three days, the morphology of LM@ZrO$_2$ NPs unchanged, while LM NPs were oxidized and changed in water (Figure S3). And the hydrated particle size of LM NPs increased significantly (Figure S4). The result confirmed that the stability of LM NPs was enhanced after ZrO$_2$ was coated to form core-shell structure. It can be seen from Fig. 1e that UV-Vis absorption spectrum of LM@ZrO$_2$ was shown absorption from 200 to 800 nm, similar to LM, indicating good potential application in the thermal therapy of tumor (Figure 1e). In order to enhance biocompatibility, PEG-SH$_{5000}$ was chosen to modify the surface of LM@ZrO$_2$ NPs.[15-17] After PEG modification, the potential of LM@ZrO$_2$ NPs was decreased from 19.4 to 5.2 mV (Figure S5a, b), which means that PEG was successfully decorated. The morphological, elemental, potential and spectroscopy measurements was clearly manifested that LM@pZrO$_2$ NPs were successfully synthesized.

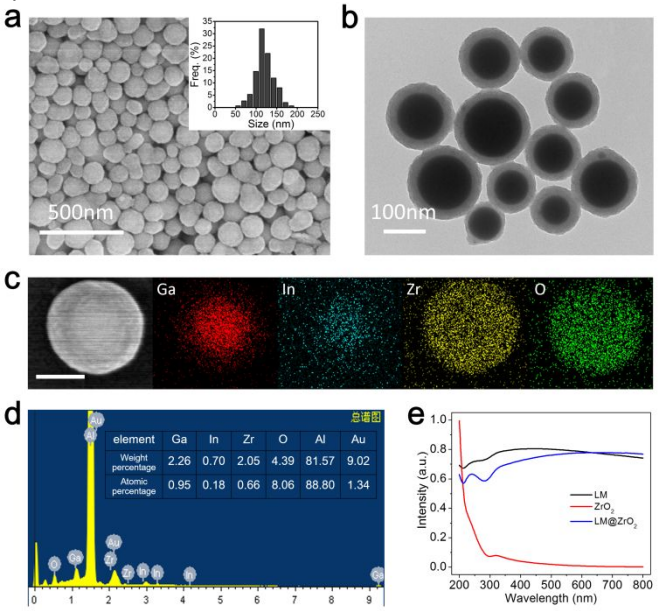

Figure 1. Characterization of LM@ZrO$_2$ NPs. a) SEM image and particle size calculated from the image of LM@ZrO$_2$ NPs. b) TEM image of LM@ZrO$_2$ NPs. c) SEM/EDS mapping and d) element content of LM@ZrO$_2$ NPs. The scale bar was 100 nm. e) UV-Vis absorption spectrum of LM NPs, ZrO$_2$ NPs and LM@ZrO$_2$ NPs.

Mechanical properties of LM@ZrO$_2$ NPs

The interaction between solid nanoparticles and cells can affect the diagnosis and treatment of various diseases.[18, 19] As an ideal drug carrier for cancer treatment, the obtained materials were hoped to be ingested by tumor cells as much as possible to achieve better therapeutic effects.[20] Previous results demonstrated that cellular uptake of particles is closely related to the surface chemistry, shape and size of the particles.[21, 22] Recently, Sun et al proved that stiffness and deformability are another parameters that have been known and proved to strongly affect the uptake of particles.[23] Soft nanoparticles accumulated more in tumor cells than rigid ones.[24, 25] Typically, stiffness was characterized by young's modulus. Inspired by literature, scanning probe microscope

was employed to test the mechanical properties of LM@ZrO_2 NPs to characterize their stiffness and deformability.[26] The young's modulus of hollow ZrO_2 NPs, LM NPs and LM@ZrO_2 NPs were measured to analyze mechanical properties of LM@ZrO_2 NPs, thus inferring the condition of LM@ZrO_2 NPs when they were internalized into cells. The quantitative nanomechanical mappings of these materials were plotted to visually show their modulus distribution (**Figure 2**a). The young's modulus of LM@ZrO_2 NPs was measured to be 357.3 MPa, which was lower than that of hollow ZrO_2 NPs (1548.3 MPa) and higher than that of LM NPs (104.7 MPa) (Figure 2b), that was, LM@ZrO_2 NPs were 'softer' than the former and 'harder' than the latter, clearly indicating that the mechanical properties of obtained LM@ZrO_2 NPs combined that of both. According to previous reports,[19] we hypothesized that LM@ZrO_2 NPs were more conducive to be internalized into cells under the same conditions, and we further validated this hypothesis in cell experiments.

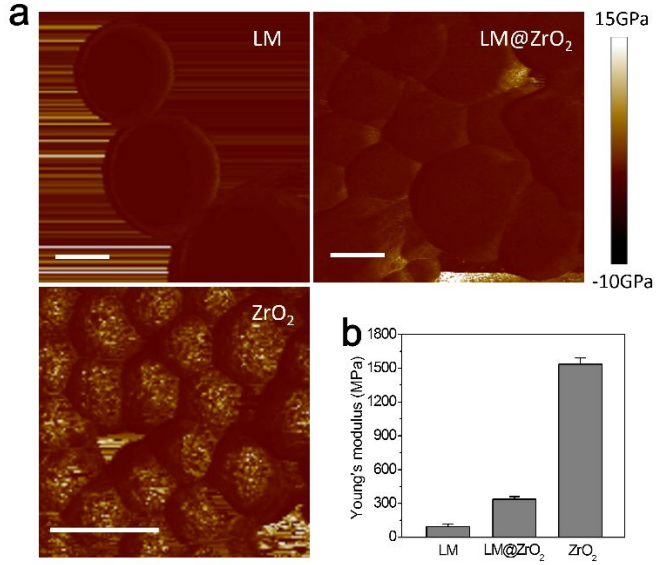

Figure 2. Mechanical properties of materials. a) Quantitative nanomechanical mappings of LM NPs, LM@ZrO_2 NPs and ZrO_2 NPs. b) Averaged young's modulus of LM NPs, LM@ZrO_2 NPs and ZrO_2 NPs. The scale bar was 200 nm.

Cytotoxicity of LM@$pZrO_2$ NPs

With the in-depth study in the biomaterials field, low toxicity of LM has been confirmed.[3, 4] However, when the size of the LM becomes small, the LM may have significantly different physiological behaviors.[8] The toxicology of LM should be further evaluated. For those reasons, PEG with good biocompatibility was modified on the obtained LM@ZrO_2NPs, and cytotoxicity experiments were carried out. HepG2 cells were incubated in culture medium with different concentrations of LM@$pZrO_2$ NPs (0, 12.5, 25, 50, 75, 100, 200 and 400 μg mL^{-1}) for 24 h, and then assayed cell viability by MTT assay. The cell viabilities with LM@$pZrO_2$ NPs at 25, 50, 100, 200 and 400 μg mL^{-1} were 88.2 %, 84.4 %, 79.7 %, 76.6 % and 74.4 %, respectively (**Figure 3**a). Although the cell activity decreased with increasing material concentration, it was still more than 70% when the concentration of LM@$pZrO_2$ NPs was as high as 400 μg mL^{-1}. The result demonstrated the low toxicity of LM@$pZrO_2$ NPs, which can be used in a series of cell experiments and was expected to be used in further animal experiments.

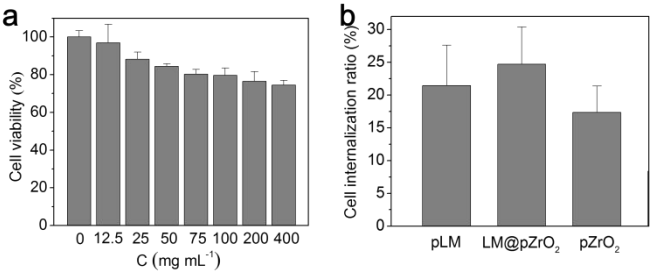

Figure 3. Cytotoxicity and internalization experience. a) Activities of HepG2 cells incubated with LM@$pZrO_2$ NPs at different concentrations (0, 12.5, 25, 50, 75, 100, 200 and 400 μg mL^{-1}) for 24h. b) After incubation with HepG2 cells for 8 hours, internalization ratio of pLM NPs, LM@$pZrO_2$ NPs and $pZrO_2$ NPs.

Internalization of LM@$pZrO_2$ NPs

Through testing the mechanical properties of materials, we have learned that the LM@ZrO_2 NPs maintained ideal deformability which was close to that of LM. And LM@ZrO_2 NPs also possesses favorable biocompatibility after PEG modification. Next, the cellular uptake experiment of the material was performed to intuitively understand whether LM@$pZrO_2$ was easily internalized into cells. Similarly, hollow ZrO_2 NPs and LM NPs were modified with PEG and used as control. HepG2 cells were incubated with 50 μg mL^{-1} these materials for 8 hours. These materials without being ingested by cells were washed out, and the cells were digested for ICP test. From the ICP results (Figure 3b), compared to the control, LM@$pZrO_2$ NPs were the most abundant in cells, that was, LM@$pZrO_2$ NPs were internalized into cells more efficiently and rapidly. This was because that LM@$pZrO_2$ NPs were softer than hollow $pZrO_2$ NPs according to their mechanical properties. Although young's modulus of LM were lower than LM@ZrO_2 NPs, pLM NPs were easier to agglomerate and combine together, resulting in less internalized than LM@$pZrO_2$ NPs. The result confirmed that LM coated with ZrO_2 was better internalized.

PT conversion performance of LM@ZrO_2 NPs

Photothermal therapy (PTT) is an emerging treatment method for cancer, mainly relying on NIR with good permeability for biological tissues to irradiate PT conversion reagents, thereby generate 'high fever' at local locations and induce cancer cell death and necrosis.[27] This technology has been extremely favored by scientists because of its simplicity, controllability and less side effects.[28-32] Recently, it has been reported that LM droplet surface can be heated rapidly under NIR radiation.[6, 7, 33] For this property, LM can be employed as a photosensitizer for PTT. Here, we tested PT conversion performance of LM@ZrO_2 NPs. 808 nm NIR laser light (1.8W) was used to investigate PT performance of LM@ZrO_2 NPs. 1 mL LM@ZrO_2 NPs with different concentration (0, 100, 300 and 500 μg mL^{-1}, dispersed in water) was added to vessel.

During 5 min radiation time, the temperature variations of the solution dispersed LM@ZrO_2 NPs were recorded by near infrared imager. From **Figure 4**a, we

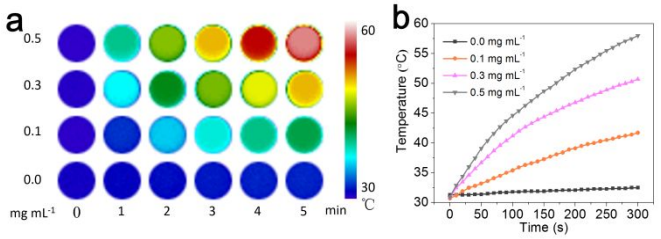

Figure 4. PT conversion performance of LM@ZrO_2 NPs. a) Temperature distribution of the cross section of the solution dispersed LM@ZrO_2 NPs. b) Temperature curves of variations at the concentrations of 0, 100, 300 and 500 μg mL^{-1}.

could observe the temperature distribution of the cross section of the solution dispersed LM@ZrO_2 NPs in the container every minute. Figure 4b showed the temperatures of the solution with LM@ZrO_2 NPs at concentration of 0, 100, 300 and 500 μg mL^{-1} were 32.5, 41.7, 50.7 and 58.0 °C after NIR radiation, respectively, which were demonstrated that the temperature of our LM nanoparticles rose, and the greater LM@ZrO_2 NPs concentration, the more obvious temperature change. For instance, the temperature variations of the solution at the concentrations of 100, 300 and 500 μg mL^{-1} were 11.0, 19.9, and 27.1 °C under the same conditions, respectively, while the change of the control group (0 μg mL^{-1}) was only 1.2 °C (Figure S6). Next, the photothermal stability were investigated with a 808 nm NIR laser irradiation for 5 min. The temperature of the LM@ZrO_2 NCs solution (500 μg mL^{-1}) increased by 27.3°C within 5 min (Figure S7). Repeat the above operations five times, the test results were basically identical. Therefore, LM@ZrO_2 NCs possesses excellent photothermal stability. Obviously, obtained LM@ZrO_2 NPs possessed efficient PT conversion performance and the potential as photosensitizers for PTT.

Cell therapy experiment

LM@$pZrO_2$ NPs not only had favorable biocompatibility, but also can be effectively uptake by cells, and had a reasonable PT conversion performance, which means that LM@$pZrO_2$ NPs can be employed for PTT. Therefore, the inactivation effect of LM@$pZrO_2$ NPs on cancer cells under NIR radiation was evaluated first. HepG2 cells were incubated with LM@$pZrO_2$ NPs at different concentrations (0, 50, 100 and 200 μg mL^{-1}) for 12 hours. Then, the cells were irradiated by NIR for 5 min. After a 24 h of incubation time, cell viability was measured. Obviously, cell activity decreased as the concentration of LM@$pZrO_2$ NPs increased. The activity of cells incubated with 200 μg mL^{-1} LM@$pZrO_2$ NPs was 30.9 % (**Figure 5**a). Next, HepG2 cells were

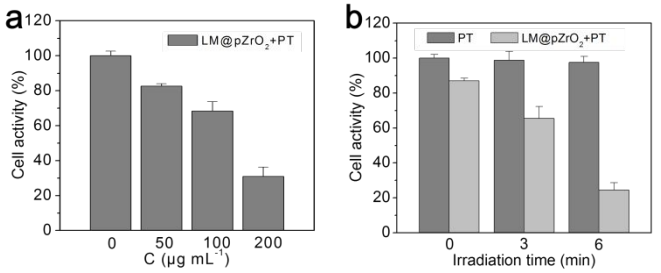

Figure 5. Cell therapy experiment. a) Activities of HepG2 cells incubated with LM@$pZrO_2$ NPs at different concentrations (0, 50, 100 and 200 μg mL^{-1}) after NIR radiation for 5 min. b) Activities of HepG2 cells incubated with 200 μg mL^{-1} LM@$pZrO_2$ NPs after NIR radiation for 0, 3 and 6 min.

incubated with 200 μg mL^{-1} LM@$pZrO_2$ NPs for 12 hours, with NIR radiation for different time. The activities of cells under NIR radiation for 0, 3 and 6 min were 87.0 %, 65.3 % and 24.4 %, respectively (Figure 5b). The cell activity incubated with LM@$pZrO_2$ NPs decreased as radiation time increased. While, there was only a slight change in the cell viability of the control group. The cell activity of the control group were 100 %, 98.7 % and 97.6 %, respectively, when the cells were irradiated by NIR radiation for 0, 3 and 6 min. In the live/dead cells staining, the cells incubated with LM@$pZrO_2$ were almost dead under NIR irradiation as well (Figure S8). These cell experiments confirmed that LM@$pZrO_2$ NPs could damage cancer cells under NIR radiation and could be further used to treat tumors.

CT imaging experiment

This study was performed in strict accordance with the NIH guidelines for the care and use of laboratory animals (NIH Publication No. 85-23 Rev. 1985) and was approved by the Institutional Animal Care and Use Committee (IACUC) of the Chinese PLA General Hospital Animal Care and Use Committee. In the cancer treatment, it is hoped that a therapeutic agent can not only cure the cancer well, but also have many functions, such as diagnostic guidance. The combination of treatment and diagnosis provides excellent cancer control and minimal side effects.[34] Thereinto, therapeutic agents for imaging-guided therapy have aroused great interest.[35-39] Yu *et al* developed a series of imaging-guided therapeutic agents, which can be applied in magnetic resonance imaging, photoacoustic tomography, photothermal therapy, or CT imaging.[40-42] CT imaging has obvious advantages in accurate diagnosis results, high image resolution and diagnostic efficiency. Zr as CT contrast agent has a favorable application prospect because of its high atomic number and mass.[43-44] Hence, CT imaging experiments were designed to evaluate the enhancement effect of LM@$pZrO_2$ NPs on CT imaging. LM@ZrO_2 NPs with different concentrations (1, 4, 8, 12, 16 and 20 mg mL^{-1}) were used for imaging experiments *in vitro*. It was clearly seen in the Figure S9a that the material concentration was linear with the CT value. The linear regression function was y = 12.4249 + 29.59317 x. The higher the material concentration, the higher the CT value and the brighter the CT image. Meanwhile, CT imaging experiments *in vivo* were designed. CT values of tumors in mice were observed at 0, 3, 6 and 9 h after LM@$pZrO_2$ NPs were injected into tail vein. As shown in the Figure S9b, the CT value of the tumor site changed with time, which verified that LM@$pZrO_2$ NPs can be used as contrast agent *in vivo*. Moreover, the CT value reached the maximum at 6h and then decreased, indicating that LM@$pZrO_2$ NPs accumulated most in the 6th hour after intravenous injection.

Anti-tumor experiment *in vivo*

After a series of *in vitro* and *in vivo* experiments, LM@$pZrO_2$ NPs were considered suitable for further PTT. The mice were divided into four groups (control group, LM@$pZrO_2$ group, PT group and LM@$pZrO_2$ + PT group) with three mice in each group. According to the results of *in vivo* CT experiments, that was, LM@$pZrO_2$ NPs accumulated most at the tumor site in the 6th hour after intravenous injection, PTT was implemented to mice at the 6th hour after administration, and surface temperature of mice was monitored by infrared thermal imaging. It could be clearly seen from the **Figure 6**a and b that the temperature of

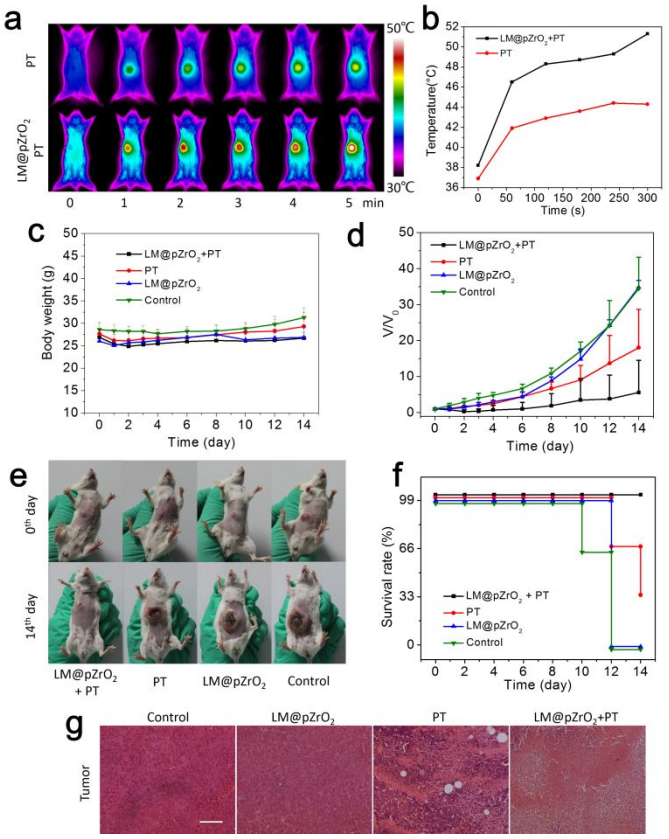

Figure 6. Anti-tumor experiment. a) Infrared imaging temperature distribution map of mice surface radiated by NIR laser per minute during PTT. b) The diagram based on the temperature of the tumor site in a). c) The diagram of body weight and d) tumor volume in different groups of mice during the anti-tumor experiment within 14 days. e) Photographs of mice on days 0 and 14 in the anti-tumor experiment. f) Survival rate of mice within 14 days. When the tumor volume was larger than 2 cm^3, the mice were considered dead. g) Tissue section of tumor in LM@$pZrO_2$ + PT group by paraffin fixation and HE staining. The scale bar was 50 μm.

mice tumors increased gradually under NIR radiation. And the tumor temperature elevation of mice (13.1 °C) injected with LM@$pZrO_2$ NPs was 5.6 °C higher than that of mice (7.5 °C) without injection, which corresponded to the ideal PT conversion performance of LM@$pZrO_2$. In the following two weeks, the body weight and tumor volume of mice in each group were recorded. As shown in the Figure 6c, the weight of the mice decreased slightly in the first two days, then it increased, and the overall change was not significant. However, the volume change of the tumors was obvious (Figure 6d). After PTT, the tumor volume of LM@$pZrO_2$ + PT group mice decreased and later increased slowly. However, the tumor volume of PT group mice increased rapidly, because the temperature of tumor was not high enough under NIR radiation and only some cancer cells were killed. The mice of LM@$pZrO_2$ group and control group showed the fastest growth in tumor volume. In Figure 6e, tumor changes on day 0 and day 14 of each group mice could be visually observed. If mice with a tumor volume of more than 2 cm^3 were considered dead, on day 14, the survival rates of mice in the control group, LM@$pZrO_2$ group, PT group and LM@$pZrO_2$ + PT group were 0%, 33.3%, 66.7% and 100%, respectively (Figure 6f). Further evaluation of the survival rate of mice treated with nanoparticles is important, and it will be studied in our follow-up work. It is worth mentioning that one mouse in the LM@$pZrO_2$ + PT group was completely cured. The inhibition rate of LM@$pZrO_2$ NPs was 91.6%, according to the tumors weight (Figure S10). The photographs of the tissue sections of the mice after sacrifice were observed (Figure S11). There were no obvious abnormalities in heart, liver, spleen, lung and kidney of mice in each group. And the most necrotic tumor cells were found in LM@$pZrO_2$ + PT group (Figure 6g). The results indicated LM@$pZrO_2$ NPs have ideal anti-tumor effect under NIR radiation.

Toxicity of LM@$pZrO_2$ NPs

Although the cytotoxicity test has confirmed the low toxicity of LM@$pZrO_2$ NPs, in order to evaluate more safety indicators *in vivo*, a toxicity experiment was designed. The distribution of LM@$pZrO_2$ NPs *in vivo* was measured by ICP (Figure S12). The toxicity of LM@$pZrO_2$ NPs was evaluated by injecting a certain amount of LM@$pZrO_2$ NPs into tail vein, observing mice for a period of time, and then testing blood and observing tissues. Mice were injected with LM@$pZrO_2$ NPs at different doses (0, 50, 100, 150 and 200 mg kg^{-1}) *via* tail vein, and each dose with three mice. During the two weeks of feeding, the mice in each group were in good health and their body weight basically showed an upward trend (Figure S13). Whereafter, the blood of the mice was tested, and the organs were taken out and observed by paraffin section and HE staining. From tests of blood routine and blood biochemistry, it was found that the index of the mice injected LM@$pZrO_2$ NPs was basically the same as that of the control group, and the difference was within the allowable range (Figure S14). Meanwhile, there was no obvious abnormality in staining sections of heart, liver, spleen, lung and kidney (**Figure 7**). The results demonstrated that the injected dose was up to 200 mg kg^{-1}, the mice still remain healthy, and LM@$pZrO_2$ NPs had good biocompatibility *in vivo*.

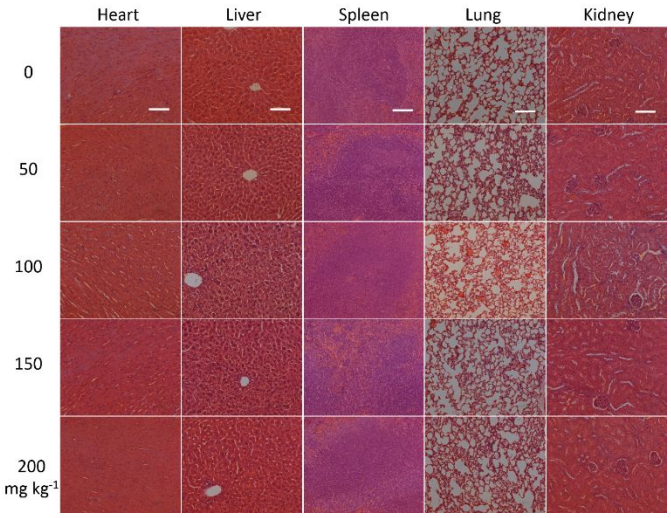

Figure 7. Tissue section (including heart, liver, spleen, lung and kidney) of mice after tail vein injection of LM@pZrO_2 NPs at different doses (0, 50, 100, 150 and 200 mg kg^{-1}) for 14 days by paraffin fixation and HE staining. The scale bar was 50 μm.

Conclusions

In summary, ZrO_2 was successfully coated on LM nanoparticles to form a stable core-shell nanostructure. Obtained nanoparticles still showed favorable flexibility, which was beneficial for effective internalization by cells. LM@pZrO_2 NPs were applied to PTT and achieved favorable results. The young's modulus of LM@ZrO_2 NPs was closed to that of LM, which was significantly lower than that of hollow ZrO_2. That was, LM@ZrO_2 NPs were 'softer' than the former and 'harder' than the latter. In internalization experiment, compared to pLM NPs and hollow pZrO_2 NPs, LM@pZrO_2 NPs were internalized into HepG2 cells more efficiently and rapidly. LM@ZrO_2 NPs were also confirmed that possessed good PT conversion performance, and low toxicity after PEG modification by cytotoxicity and toxicity experiments. In cell therapy experiments and anti-tumor experiment *in vivo*, LM@pZrO_2 NPs could damage cancer cells and mice tumors under NIR radiation. The activity of HepG2 cells incubated with 200 μg mL^{-1} LM@pZrO_2 NPs under NIR radiation for 9 min was less than 22%. Tumor inhibition rate of mice was 91.6%, and one mouse in the LM@pZrO_2 + PT group was completely cured. In addition, LM@pZrO_2 had the ability of CT imaging and could be used for CT imaging *in vivo*. This research provides a promising vehicle for nanotheranostics by a core-shell LM nanostructure, holding the significant advantages of stability as well as flexibility.

Conflicts of interest

There are no conflicts to declare.

Acknowledgements

The authors acknowledge financial support from the National Natural Science Foundation of China (Nos. 61671435, 81630053), CAS-DOE program (No. GJHZ1705).

Notes and references

1 M. D. Dickey, *ACS Appl Mater Inter*, 2014, **6**, 18369-18379.
2 M. D. Dickey, *Adv Mater*, 2017, **29**.
3 L. Yi and J. Liu, *Int Mater Rev*, 2017, **62**, 415-440.
4 L. Yi, C. Jin, L. Wang and J. Liu, *Biomaterials*, 2014, **35**, 9789-9801.
5 T. Daeneke, K. Khoshmanesh, N. Mahmood, I. A. de Castro, D. Esrafilzadeh, S. J. Barrow, M. D. Dickey and K. Kalantar-Zadeh, *Chem Soc Rev*, 2018, **47**, 4073-4111.
6 Y. Lu, Y. Lin, Z. Chen, Q. Hu, Y. Liu, S. Yu, W. Gao, M. D. Dickey and Z. Gu, *Nano Lett*, 2017, **17**, 2138-2145.
7 S. A. Chechetka, Y. Yu, X. Zhen, M. Pramanik, K. Pu and E. Miyako, *Nat Commun*, 2017, **8**, 15432.
8 J. Yan, Y. Lu, G. Chen, M. Yang and Z. Gu, *Chem Soc Rev*, 2018, **47**, 2518-2533.
9 O. V. Kharissova, B. I. Kharisov, T. H. García and U. O. Méndez, *Synthesis and Reactivity in Inorganic, Metal-Organic, and Nano-Metal Chem*, 2009, **39**, 662-684.
10 K. Chatterjee, S. Sarkar, K. Jagajjanani Rao and S. Paria, *Adv Colloid Interface Sci*, 2014, **209**, 8-39.
11 L. Labrador-Paez, E. C. Ximendes, P. Rodriguez-Sevilla, D. H. Ortgies, U. Rocha, C. Jacinto, E. Martin Rodriguez, P. Haro-Gonzalez and D. Jaque, *Nanoscale*, 2018, **10**, 12935-12956.
12 F. Wang, C. Li, J. Cheng and Z. Yuan, *Int J Env Res Pub He*, 2016, **13**.
13 Z. Wu, S. Yang and W. Wu, *Nanoscale*, 2016, **8**, 1237-1259.
14 H. Shi, M. Niu, L. Tan, T. Liu, H. Shao, C. Fu, X. Ren, T. Ma, J. Ren, L. Li, H. Liu, K. Xu, J. Wang, F. Tang and X. Meng, *Chem Sci*, 2015, **6**, 5016-5026.
15 L. Xu, J. Yang, B. Xue, C. Zhang, L. Shi, C. Wu, Y. Su, X. Jin, Y. Liu and X. Zhu, *Biomaterials*, 2017, **147**, 1-13.
16 H. Otsuka, Y. Nagasaki and K. Kataoka, *Adv Drug Deliver Rev*, 2012, **64**, 246-255.
17 G. Pasut and F. M. Veronese, *J Control Release*, 2012, **161**, 461-472.
18 X. Yi, X. Shi and H. Gao, *Phys Rev Lett*, 2011, **107**, 098101.
19 Z. Teng, C. Wang, Y. Tang, W. Li, L. Bao, X. Zhang, X. Su, F. Zhang, J. Zhang, S. Wang, D. Zhao and G. Lu, *J Am Chem Soc*, 2018, **140**, 1385-1393.
20 J. Zhao and M. H. Stenzel, *Polym Chem*, 2018, **9**, 259-272.
21 Z. Motao, N. Guangjun, M. Huan, X. Tian, N. Andre and Z. Yuliang, *Acc Chem Res*, 2013, **46**, 622-631.
22 C. M. Beddoes, C. P. Case and W. H. Briscoe, *Adv Colloid Interface Sci*, 2015, **218**, 48-68.
23 H. Sun, M. Björnmalm, J. Cui, E. H. H. Wong, Y. Dai, Q. Dai, G. G. Qiao and F. Caruso, *ACS Macro Lett*, 2015, **4**, 1205-1209.
24 H. Sun, E. H. H. Wong, Y. Yan, J. Cui, Q. Dai, J. Guo, G. G. Qiao and F. Caruso, *Chem Sci*, 2015, **6**, 3505-3514.
25 Z. Sulin, G. Huajian and B. Gang, *Acs Nano*, 2015, **9**, 8655-8671.
26 Y. Liu, B. Workalemahu and X. Jiang, *Small*, 2017, **13**, 1701815.
27 J. Chen, C. Ning, Z. Zhou, P. Yu, Y. Zhu, G. Tan and C. Mao, *Prog Mater Sci*, 2019, **99**, 1-26.
28 L. Zou, H. Wang, B. He, L. Zeng, T. Tan, H. Cao, X. He, Z. Zhang, S. Guo and Y. Li, *Theranostics*, 2016, **6**, 762-772.
29 N. S. Abadeer and C. J. Murphy, *The Journal of Physical Chemistry C*, 2016, **120**, 4691-4716.
30 S. Tang, M. Chen and N. Zheng, *Small*, 2014, **10**, 3139-3144.
31 Y. He, W. Cao, C. Cong, X. Zhang, L. Luo, L. Li, H. Cui and D. Gao, *ACS Sustain Chem Eng*, 2019, **7**, 3584-3592.

32 X. Zhang, L. Luo, L. Li, Y. He, W. Cao, H. Liu, K. Niu and D. Gao, *Nanomedicine*, 2019, **15**, 142-152.
33 Y. Lu, Q. Hu, Y. Lin, D. B. Pacardo, C. Wang, W. Sun, F. S. Ligler, M. D. Dickey and Z. Gu, *Nat Commun*, 2015, **6**, 10066.
34 E. K. Lim, T. Kim, S. Paik, S. Haam, Y. M. Huh and K. Lee, *Chem Rev*, 2015, **115**, 327-394.
35 Q. Wu, J. Yu, M. Li, L. Tan, X. Ren, C. Fu, Z. Chen, F. Cao, J. Ren, L. Li, P. Liang, Y. Zhang and X. Meng, *Biomaterials*, 2018, **179**, 122-133.
36 M. S. Muthu, D. T. Leong, L. Mei and S. S. Feng, *Theranostics*, 2014, **4**, 660-677.
37 J. Ge, Q. Jia, W. Liu, L. Guo, Q. Liu, M. Lan, H. Zhang, X. Meng and P. Wang, *Adv Mater*, 2015, **27**, 4169-4177.
38 C. M. Hessel, V. P. Pattani, M. Rasch, M. G. Panthani, B. Koo, J. W. Tunnell and B. A. Korgel, *Nano Lett*, 2011, **11**, 2560-2566.
39 Z. Wang, Y. Ju, S. Tong, H. Zhang, L. Jian, B. Wang and Y. Hou, *Nanoscale Horiz*, 2018, **3**, 10.1039.C1038NH00135A-.
40 Y. Jing, Y. Ce, L. Jingdingsha, D. Yichen, Z. Lei, Y. Muhammad Zubair, L. Jian, P. Rui, W. Lanbin and X. Lili, *Adv Mater*, 2014, **26**, 4114.
41 J. Yu, Y. Ju, L. Zhao, X. Chu, W. Yang, Y. Tian, F. Sheng, L. Zhang, J. Lin and F. Liu, *Acs Nano*, 2015, **10**, 159.
42 Y. Ju, H. Zhang, J. Yu, S. Tong, N. Tian, Z. Wang, X. Wang, X. Su, X. Chu and J. Lin, *Acs Nano*, 2017, **11**, 9239.
43 E. W. Price and C. Orvig, *Chem Soc Rev*, 2014, **43**, 260-290.
44 Z. Chen, M. Niu, G. Chen, Q. Wu, L. Tan, C. Fu, X. Ren, H. Zhong, K. Xu and X. Meng, *ACS Nano*, 2018, DOI: 10.1021/acsnano.8b07749.

TOC

The nanoparticle not only formed a stable LM core-shell structure, but also maintained the ideal flexibility of LM.